2004-01-2218

Quantitative Evaluation of Fatigue Crack Growth Retardation Due to Crack Branching

Marco Antonio Meggiolaro
Mechanical Engineering Department
Pontifical Catholic University of Rio de Janeiro (PUC-Rio), Brazil

Antonio Carlos de Oliveira Miranda
Tecgraf - Computer Graphics Technology Group
Pontifical Catholic University of Rio de Janeiro (PUC-Rio), Brazil

Jaime Tupiassú Pinho de Castro
Mechanical Engineering Department
Pontifical Catholic University of Rio de Janeiro (PUC-Rio), Brazil

Luiz Fernando Martha
Civil Engineering Department
Pontifical Catholic University of Rio de Janeiro (PUC-Rio), Brazil

e-mails: meggi@mec.puc-rio.br, amiranda@tecgraf.puc-rio.br, jtcastro@mec.puc-rio.br, lfm@civ.puc-rio.br

ABSTRACT

Fatigue crack kinking and bifurcation are phenomena capable of inducing significant growth retardation or even crack arrest. However, bifurcated crack models available in the literature cannot account for the subsequent propagation behavior observed in practice. In this work, specialized Finite Element (FE) and life assessment software are used to predict the reduction in the propagation rates in kinked and bifurcated cracks. The crack path and associated stress intensity factors (SIF) of bifurcated cracks are numerically obtained for several bifurcation angles and branch lengths. From these results, empirical crack retardation equations are proposed to model the retardation factor along the crack path, allowing for a better understanding of the influence of crack deflection in the propagation life.

Keywords: fatigue, crack bifurcation, growth retardation.

INTRODUCTION

Overloads, multi-axial stresses, microstructural inhomogeneities such as grain boundaries and interfaces, or environment effects can significantly deviate fatigue cracks from their Mode I growth direction, generating crack kinking or branching [1]. A fatigue crack deviated from its nominal Mode I plane induces mixed-mode near-tip conditions even if the far-field stress is purely Mode I. Since the stress intensity factors (SIF) associated to deflected or branched fatigue cracks can be considerably smaller than that of a straight crack with the same projected length, such deviations can cause retardation or even arrest of crack growth [2]. Very small differences between the branch lengths b and c are enough to cause the shorter branch to arrest as the larger one propagates, until reaching approximately its pre-overload SIF and growth rate. This typical propagation behavior has been observed on a branched crack on an aircraft wheel rim made of 2014-T6 aluminum alloy [3].

Analytical solutions have been obtained for the SIF of kinked and branched cracks [2, 4-8]. However, numerical methods such as Finite Elements (FE) and Boundary Elements (BE) are the only means to predict the subsequent curved propagation behavior.

To predict the path of a branched crack and to calculate the associated Modes I and II SIF, an interactive FE program named Quebra2D is used [9]. This program simulates two-dimensional fracture processes based on a

FE self-adaptive strategy, using appropriate crack tip elements and crack increment criteria. The adaptive FE analyses are coupled with modern and efficient automatic remeshing schemes. The program has been validated through experiments on ESE(T) and modified C(T) specimens made of 4340 and 1020 steel, and from comparisons with analytical solutions for kinked cracks. The crack path and associated SIF are then exported to **ViDa**, a general-purpose fatigue design program developed to predict both initiation and propagation fatigue lives under variable loading by all classical design methods [10]. This companion life assessment program is used to estimate the number of delay cycles associated with crack bifurcation. In the next sections, the propagation behavior of kinked and bifurcated (branched) cracks is calculated.

MIXED-MODE CRACK GROWTH CALCULATIONS

In mixed-mode crack growth calculations using FE, three methods are generally used to compute the stress intensity factors along the (generally curved) crack path: the displacement correlation technique [11], the potential energy release rate computed by means of a modified crack-closure integral technique [12-13], and the J-integral computed by means of the equivalent domain integral (EDI) together with a mode decomposition scheme [14-15]. The EDI method replaces the J-integral along a contour by another one over a finite size domain, using the divergence theorem, which is more convenient for FE analysis. Since Bittencourt et al. [16] showed that for sufficiently refined FE meshes all three methods predict essentially the same results, only the EDI method is considered in the calculations presented here. However, the other two methods also provide good results even for coarse meshes.

Several models have been proposed to obtain an equivalent SIF K_{eq} from K_I, K_{II} and K_{III}. Tanaka [18] obtained an equivalent stress intensity model based on the displacements behind the crack tip reaching a critical value, leading to

$$K_{eq} = \left[K_I^4 + 8 \cdot K_{II}^4 + \frac{8 \cdot K_{III}^4}{1-\nu} \right]^{0.25} \tag{1}$$

where ν is Poisson's coefficient.

Hussain et al. [19] used complex variable mapping functions to obtain the potential energy release rate $\mathcal{G}$ at a direction θ with respect to the crack propagation plane. He assumed that crack extension occurs in a direction $\theta = \theta_0$ that maximizes $\mathcal{G}$, leading to the maximum fracturing energy release rate ($\mathcal{G}_{max}$) criterion. Thus, an equivalent SIF is obtained at $\theta = \theta_0$ that maximizes the expression

$$K_{eq} = \sqrt{\begin{aligned} &\frac{4}{(3+\cos^2\theta)^2}\left(\frac{1-\theta/\pi}{1+\theta/\pi}\right)^{\theta/\pi}[(1+3\cos^2\theta)K_I^2 + \\ &-8\sin\theta\cos\theta \cdot K_I K_{II} + (9-5\cos^2\theta)K_{II}^2] \end{aligned}} \tag{2}$$

The computed θ_0 values at each calculation step are used to obtain the crack incremental growth direction - and thus the fatigue crack path - in the linear-elastic regime.

Sih [20] proposed a criterion for mixed-mode loading based on the strain energy density S around the crack tip. It is assumed that the crack propagates in a direction $\theta = \theta_0'$ that minimizes S. The associated equivalent SIF is then calculated at $\theta = \theta_0'$ that minimizes the expression

$$\begin{aligned} K_{eq}^2 = \frac{1}{4(1-2\nu)} &\{(3-4\nu-\cos\theta)(1+\cos\theta)\cdot K_I^2 + \\ &+ 2\sin\theta\cdot[\cos\theta - 1 + 2\nu]\cdot K_I K_{II} + \\ &+ [4(1-\nu)(1-\cos\theta) + (1+\cos\theta)(3\cos\theta-1)]\cdot K_{II}^2 + \\ &+ 4K_{III}^2\} \end{aligned} \tag{3}$$

Erdogan and Sih [21] proposed the maximum circumferential stress ($\sigma_{\theta max}$) criterion, which considers that crack growth should occur in the direction that maximizes the circumferential stress in the region close to the crack tip. They considered the stresses at the crack tip under combined Mode I and II loading, given by summing up the stress fields generated by each mode:

$$\sigma_r = \frac{1}{\sqrt{2\pi r}}\left\{\begin{aligned} &\frac{1}{4}\left(5\cos\frac{\theta}{2} - \cos\frac{3\theta}{2}\right)\cdot K_I + \\ &-\frac{1}{4}\left(5\sin\frac{\theta}{2} - 3\sin\frac{3\theta}{2}\right)\cdot K_{II} \end{aligned}\right\} \tag{4}$$

$$\sigma_\theta = \frac{1}{\sqrt{2\pi r}}\left\{\begin{aligned} &\frac{1}{4}\left(3\cos\frac{\theta}{2} + \cos\frac{3\theta}{2}\right)\cdot K_I + \\ &-\frac{3}{4}\left(\sin\frac{\theta}{2} + \sin\frac{3\theta}{2}\right)\cdot K_{II} \end{aligned}\right\} \tag{5}$$

$$\tau_{r\theta} = \frac{1}{\sqrt{2\pi r}}\left\{\begin{aligned} &\frac{1}{4}\left(\sin\frac{\theta}{2} + \sin\frac{3\theta}{2}\right)\cdot K_I + \\ &+\frac{1}{4}\left(\cos\frac{\theta}{2} + 3\cos\frac{3\theta}{2}\right)\cdot K_{II} \end{aligned}\right\} = -\frac{2}{3}\frac{\partial\sigma_\theta}{\partial\theta} \tag{6}$$

where σ_r is the normal stress component in the radial direction, σ_θ is the normal stress component in the tangential direction and $\tau_{r\theta}$ is the shear stress component. These expressions are valid both for plane stress and plane strain. The Maximum Circumferential Stress criterion assumes that crack growth begins on a plane perpendicular to the direction in which σ_θ is maximum. The maximum value of σ_θ is obtained when $\partial\sigma_\theta/\partial\theta$ is zero, which is equivalent to equating $\tau_{r\theta} = 0$, according to Equation (6). The equation $\tau_{r\theta} = 0$ has a trivial solution $\theta = \pm\pi$ (for $\cos(\theta/2) = 0$), and a non-trivial solution $\theta = \theta_0$" given by

$$\theta_0" = 2\arctan\left(\frac{1}{4}\frac{K_I}{K_{II}} \pm \frac{1}{4}\sqrt{\left(\frac{K_I}{K_{II}}\right)^2 + 8}\right) \quad (7)$$

where the sign of θ_0" is the opposite of the sign of K_{II}. According to the $\sigma_{\theta max}$ criterion, the equivalent SIF is calculated at the value $\theta = \theta_0$", which maximizes the expression

$$K_{eq} = \frac{1}{4}\left(3\cos\frac{\theta}{2} + \cos\frac{3\theta}{2}\right)\cdot K_I - \frac{3}{4}\left(\sin\frac{\theta}{2} + \sin\frac{3\theta}{2}\right)\cdot K_{II} \quad (8)$$

The above models have notable differences if the amount of Mode II loading is significant. For instance, under pure Mode II loading, the propagation angle θ is ±70.5°, ±75° and ±82° according to the $\sigma_{\theta max}$, $\mathcal{G}_{max}$ and S_{min} models, respectively, leading to K_{eq} values of approximately $1.15\cdot K_{II}$, $1.60\cdot K_{II}$ and $1.05\cdot K_{II}$ (assuming $\nu = 0.3$). In addition, Tanaka's model results in this case in $K_{eq} = 1.68\cdot K_{II}$. The values of θ and K_{eq} obtained from each model are plotted in Figures 1 and 2 as a function of the K_{II}/K_I ratio.

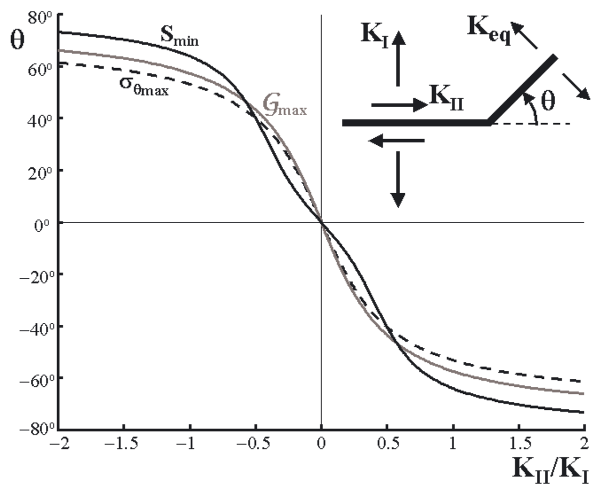

Figure 1. Crack propagation direction θ as a function of the K_{II}/K_I ratio according to the $\sigma_{\theta max}$, $\mathcal{G}_{max}$ and S_{min} models.

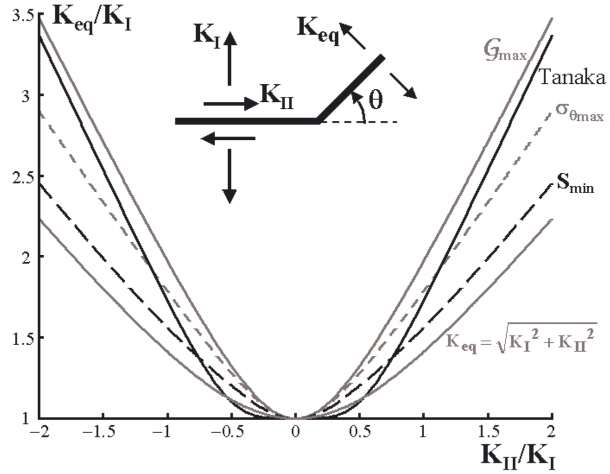

Figure 2. Equivalent SIF K_{eq} as a function of the K_{II}/K_I ratio according to several models.

The differences among the studied models might be significant for mixed-mode fracture predictions, however they are negligible for fatigue crack propagation calculations. In fact, since all above models predict crack path deviation ($\theta \neq 0$) under any K_{II} different than zero (see Figure 1), they imply that fatigue cracks will always attempt to propagate in pure Mode I, minimizing the amount of Mode II loading, curving their paths if necessary to avoid rubbing their faces. As soon as the crack path is curved to follow pure Mode I, all models agree that K_{eq} is equal to K_I. Therefore, not only the crack path but also the SIF values calculated by any of the above criteria are essentially the same. This has been verified by Bittencourt et al. [16], who concluded from FE simulations that these criteria provide basically the same numerical results. Since the Maximum Circumferential Stress criterion is the simplest, presenting a closed form solution, it is the one adopted in the present work.

CRACK BIFURCATION PREDICTIONS

In this section, the Modes I and II SIF are evaluated for cracks of length a with a small bifurcation of branch lengths b_0 and c_0 ($b_0 \geq c_0$) forming an angle 2θ, see Figure 3(a). To perform the calculations, a standard C(T) specimen is FE modeled using Quebra2D with width w = 32.0mm, crack length a = 14.9mm, and bifurcations with initial crack branch lengths b_0 = 10μm and c_0 = 5, 7, 8, 9, 9.5 and 10μm. The Modes I and II SIF k_1 and k_2 of each crack branch are obtained considering bifurcation angles 2θ between 40° and 168°. Note that typical overload-induced bifurcated cracks can have initial branch lengths between 10 and 100μm, with 2θ varying between 30°, e.g. for very brittle materials such as glass, and 180°, e.g. in the vicinity of the interface of a bi-material composite, when a crack propagates from the weak to the strong material [22].

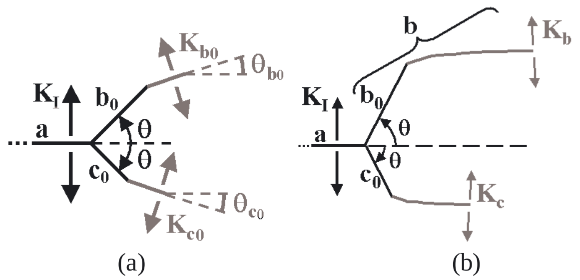

Figure 3. Schematic representation of a branched crack at the onset of propagation (a) and during propagation (b).

Note that an efficient meshing algorithm is fundamental to avoid elements with poor aspect ratio, since the ratio between the size scale of the larger and smaller elements is above 1,000 in this case. To accomplish that, Quebra2D uses an innovative algorithm incorporating a quadtree procedure to develop local guidelines to generate elements with the best possible shape. The internal nodes are generated simultaneously with the elements, using the quadtree procedure only as a node-spacing function. This approach tends to give a better control over the generated mesh quality and to decrease the amount of heuristic cleaning-up procedures. Moreover, it specifically handles discontinuities in the domain or boundary of the model. Finally, to enhance the quality of the shape of the mesh element, an *a posteriori* local mesh improvement procedure is used [23].

Figure 4 shows the FE results for the SIF k_1 and k_2 (normalized by the Mode I SIF K_I of the straight crack) of symmetrically bifurcated cracks (which have $b_0 = c_0$). Note that k_2 vanishes for a bifurcation angle $2\theta = 2\theta^* = 53^o$. The bifurcation angle $2\theta^*$ for which k_2 vanishes on a symmetrically branched crack is a very important parameter, because it is associated with a self-similar propagation of the crack branches. Since k_2 is equal to zero, no path deflection will occur in this case, thus both branches will continue propagating at an angle $\theta^* = \pm 26.5^o$ with respect to the horizontal. Note however that the value of $2\theta^*$ is a function of the ratio b_0/a. For $b_0/a < 0.001$, $2\theta^*$ tends to approximately 53^o, but for $b_0/a = 0.025$ the value of $2\theta^*$ drops to 36^o [24] and for $b_0/a = 0.1$ it has been predicted that $2\theta^* = 32^o$ [25]. Therefore, the infinitesimal kink solution shown in Figure 4 can only be numerically reproduced using very refined FE calculations with b_0/a ratios much smaller than 0.1 or 0.025, such as the considered $b_0/a = 10\mu m/14.9mm = 6.7 \cdot 10^{-4}$.

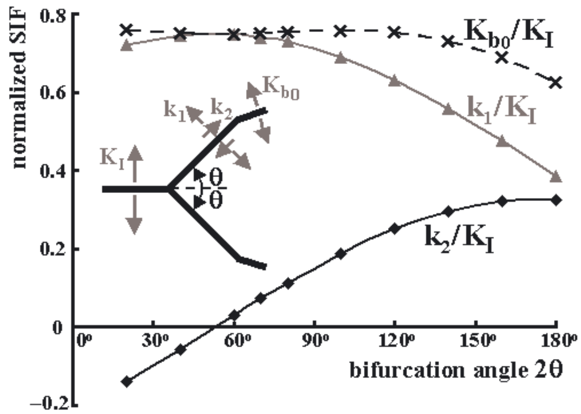

Figure 4. Normalized stress intensity factors for symmetrically bifurcated cracks.

The FE-obtained k_1 and k_2 are now used to compute, using Equation (8), an equivalent SIF K_{b0} of both branches that will characterize the propagation behavior immediately after the bifurcation event. Note from Figure 4 that K_{b0} is approximately constant for symmetrically bifurcated cracks with $2\theta < 140^o$, estimated equal to 0.75 within 3%.

Special care must be taken when calculating the SIF of bifurcated cracks with 2θ approaching 180^o. In this case, the effective SIF increases considerably at the very beginning of the propagation. For instance, a symmetrically bifurcated crack with $2\theta = 160^o$ has K_{b0}/K_I equal to 0.688 for both branches (as suggested in Figure 4), however after a brief propagation of less than $0.1 \cdot b_0$ this value jumps to 0.751. Therefore, the decrease in K_{b0} for $2\theta > 140^o$ shown in Figure 4 is only valid at the onset of propagation, almost immediately increasing to approximately 0.75 after that. It is concluded from further simulations that K_{b0} can be estimated as 0.75 within 3% for all symmetrically bifurcated cracks with $40^o \leq 2\theta \leq 168^o$.

Figure 5 shows the FE results for the equivalent SIF K_{b0} and K_{c0} of the longer and shorter branches respectively (normalized by the Mode I SIF K_I of the straight crack) of both symmetrically and asymmetrically bifurcated cracks. Note once again the apparent decrease in K_{b0} for $2\theta > 140^o$, an effect that disappears soon after the propagation starts. This high initial sensitivity can be explained by the small projected length of crack branches with 2θ approaching 180^o. This projected length is easily overcome even by a very small propagation step, significantly changing the crack geometry and SIF. For instance, it is found that a bifurcated crack with $2\theta = 170^o$ has an initial propagation angle around 35^o, thus the crack branch b_0 has the same projected length as the one generated by a propagation step of only $b_0 \cdot \cos(0.5 \cdot 170^o)/\cos(35^o) \cong 0.11 \cdot b_0$.

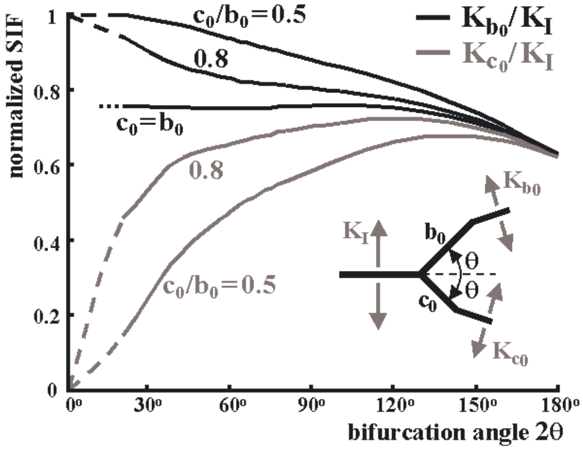

Figure 5. Normalized equivalent stress intensity factors for symmetrically and asymmetrically bifurcated cracks.

Another interesting conclusion is that the initial propagation direction of the longer branch is always below 40^o (with respect to the pre-overload growth direction), independently of the considered bifurcation angle 2θ. Therefore, for values of 2θ greater than 80^o, a sharp deflection can be clearly noted in the beginning of the propagation. This deflection has been experimentally confirmed by Lankford and Davidson [1], who carried out overload fatigue crack tests on a 6061-T6 aluminum alloy in a scanning electron microscope using a special in-situ servo-controlled hydraulic loading stage, obtaining growth retardation caused by crack bifurcation. They have found that the bifurcated crack would grow only a short distance in the same direction of the overload-induced bifurcation, before a sharp deflection in the crack path would occur. This deflection causes a sudden increase in the Mode I SIF almost immediately after the propagation begins, resulting in a significantly smaller retardation effect if compared to simplistic predictions based on branched crack solutions that do not include the propagation phase. However, if the equivalent stress intensity ranges of both branches are below the threshold SIF ΔK_{th}, then the entire crack arrests and therefore no sharp deflection has the chance to develop.

The FE-obtained results shown in Figure 5 are used to fit empirical equations to the initial SIF K_{b0} and K_{c0} of the longer and shorter branches, resulting in:

$$\frac{K_{b0}}{K_I} = 0.75 + (1 - \sin\theta) \cdot \left(1 - \frac{c_0}{b_0}\right) \qquad (9)$$

$$\frac{K_{c0}}{K_I} = 0.75 - (1 - \sin\theta) \cdot \left(1 - \frac{c_0}{b_0}\right) \qquad (10)$$

Equations (9-10) result in errors smaller than 2% for $40^o \le 2\theta \le 168^o$ and $0.7 \le c_0/b_0 \le 1.0$. Figure 6 plots the FE results against the proposed equations, showing a good fit. In the next section, further FE analyses are conducted to evaluate the subsequent propagation behavior of these bifurcated cracks.

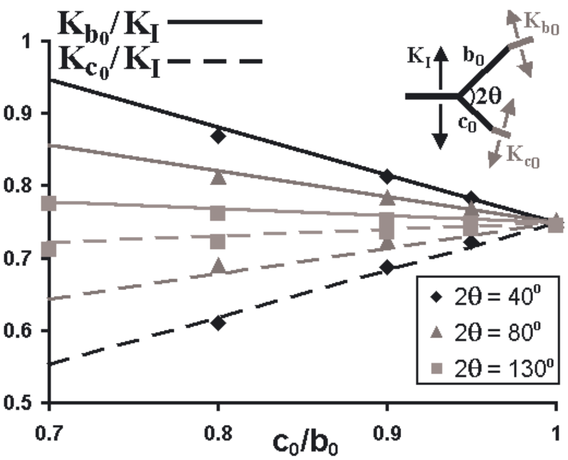

Figure 6. Initial equivalent SIF of both branches of a bifurcated crack as a function of the asymmetry ratio c_0/b_0 and bifurcation angle 2θ.

PROPAGATION OF BRANCHED CRACKS

The growth of branched cracks is studied in the Quebra2D program using the same CT specimens described above. A fixed crack growth step of $\Delta b = 3\mu m$ (or $1\mu m$ during the first propagation steps) is considered for the propagation of the longer branch b. This growth step is calculated in the direction defined by the $\sigma_{\theta max}$ criterion. Due to the differences in the crack growth rate, a growth step Δc smaller than Δb is expected for the shorter branch. This smaller step is obtained assuming a Paris crack propagation law,

$$\frac{da}{dN} = A \cdot \Delta K^m \qquad (11)$$

where A and m are material constants. If ΔK_b and ΔK_c are respectively the stress intensity ranges of the longer and shorter branches, then the growth step Δc of the shorter branch c should be

$$\Delta c = \Delta b \cdot \left(\frac{\Delta K_c}{\Delta K_b}\right)^m \qquad (12)$$

Interestingly, the ratio between the propagation rates of the two branches is independent of the material constant A. In this analysis, the exponent m is assumed to be 2.0, 3.0, and 4.0, which are representative values for steels.

Once a (small) growth step Δb is chosen for the numerical propagation of the longer branch, the growth of the shorter branch Δc is readily obtained from Equation (12). Both the crack path and the associated SIF along each branch are then obtained using the FE program. It must be noted, however, that linear-elastic FE calculations can only lead to accurate solutions if the lengths of the crack branches b and c are significantly larger than the size scale of both the microstructure and the near-tip plastic (or process) zone. But as the crack branches grow further, the FE method can give a reasonable estimate of their behavior where LEFM is applicable. In addition, the growth of branched cracks is typically transgranular, as verified from optical microscope observations performed by Shi et al. [26], which is one of the requirements to allow for the simulation of fatigue behavior in isotropic linear-elastic regime.

The propagation behavior of branched cracks is studied using FE considering no closure effects ($K_{op} = 0$). Figure 7 shows the contour plots of the stress in the load direction axis and propagation results for a bifurcated crack with angle $2\theta = 150^o$, obtained from the FE analysis for $c_0/b_0 = 0.91$, m = 2 and no closure. In this figure, the deformations are highly amplified to better visualize the crack path. Note that the crack path deviates from the original branch angles, deflecting from $\pm 75^o$ to approximately $\pm 28^o$. In addition, the originally shorter branch arrests after propagating (only) about 29µm, while the longer branch returns to the pre-overload growth direction and SIF (even though the subsequent crack growth plane may be offset from the pre-overload one, see Figure 7).

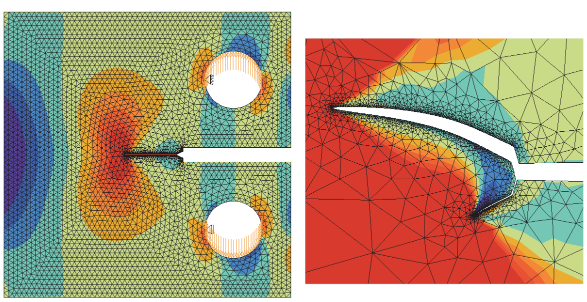

Figure 7. Propagation simulation of a bifurcated crack on a CT specimen (left), with a close-up of the two original 11µm and 10µm branches with angle $2\theta = 150^o$ (right).

Figure 8 shows the crack paths obtained from the FE analyses of bifurcated cracks with $2\theta = 130^o$ and $c_0/b_0 = \{0.5, 0.8, 0.95, 1\}$, considering m = 2 and no closure effects. The dashed lines show the theoretical propagation behavior of a perfectly symmetric bifurcation ($c_0/b_0 = 1$). In this case, the retardation effect would never end because both branches would propagate symmetrically without arresting. Clearly, such behavior is not observed in practice, since the slightest difference between b_0 and c_0 would be sufficient to induce an asymmetrical behavior.

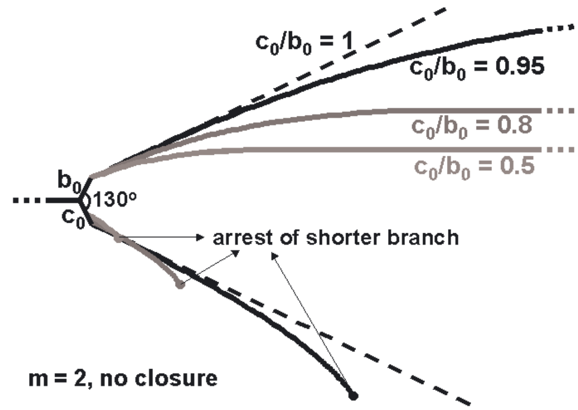

Figure 8. Bifurcated crack paths for several c_0/b_0 ratios.

The angles of the symmetrical dashed lines in Figure 8 for small b_0/a ratios are found to be $\theta^* = \pm 26.5^o$ with respect to the horizontal, where $2\theta^*$ has been previously defined as the bifurcation angle for which k_2 vanishes on a symmetrically branched crack. As the symmetrical branches grow following the $\pm 26.5^o$ directions, it is found that the ratio between the equivalent SIF and the SIF of a straight crack with same projected length is approximately constant and equal to 0.757, a value compatible with the 0.75 estimate for K_{b0}. Note that the directions $\pm 26.5^o$ are independent of 2θ and m, therefore symmetrical bifurcations with any initial angle 2θ would tend to the self-similar solution $2\theta^* = 53^o$ as long as the ratio b/a of the propagating branches is sufficiently small. FE calculations also showed that the slopes of the dashed lines are gradually decreased as both branches grow, resulting in angles $\pm 18^o$ in the vicinity of b/a = 0.025, $\pm 16^o$ close to b/a = 0.1, and $\pm 15.3^o$ for b/a >> 1. This last result has been obtained from a FE analysis of a symmetrical bifurcation starting at the edge of a very large plate (therefore with a = 0 and $b/a \rightarrow \infty$).

Figure 8 also shows that lower c_0/b_0 ratios result in premature crack arrest, leading to smaller retardation zones. Also, the propagation path of the longer branch is usually restrained to the region within the dashed lines, while the shorter one is “pushed” outside that envelope due to shielding effects.

The size of the retardation zone can be estimated from the ratio b_f/b_0, where b_f is the value of the length parameter b of the longer branch beyond which the retardation effect ends (in the same way that it was defined for kinked cracks). The ratio b_f/b_0 is then calculated through FE propagation simulations for all combinations of $c_0/b_0 = \{0.5, 0.8, 0.9, 0.95\}$, $2\theta = \{40^o, 80^o, 130^o, 168^o\}$

and m = {2, 3, 4}, and fitted by the proposed empirical function:

$$\frac{b_f}{b_o} = \exp\left(\frac{2\theta - 30^o}{56 + 17\cdot(m-2)^{2/3}}\right) / \, (1 - c_0 / b_0)^{(12-m)/20} \quad (13)$$

Figure 9 shows a comparison between the fitted and the FE-obtained data. Note that a greater symmetry between the branches (as c_0/b_0 approaches 1.0) results in a longer retardation zone, as expected from the delayed arrest of the shorter branch.

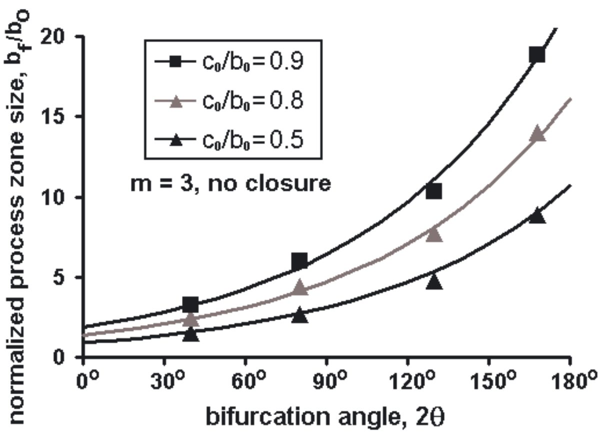

Figure 9. Normalized process zone size as a function of the bifurcation angle and branch asymmetry c_0/b_0 (m=3).

The FE-calculated equivalent SIF K_b and K_c of the longer and shorter branches are now evaluated along the obtained crack paths. Figure 10 plots the crack retardation factors (defined as the ratios between K_b or K_c and the Mode I SIF K_I of a straight crack) for $2\theta = 130^o$ and m = 2, as a function of the normalized length $(b{-}b_0)/b_0$ of the longer branch (measured along the propagation path). Because of the different crack branch lengths, the SIF at the longer is much higher than that at the shorter branch. Assuming K_b and K_c to be the crack driving force, it can be seen from Figure 10 that the longer branch reaches its minimum propagation rate right after the bifurcation occurs, returning to its pre-overload rate as the crack tip advances away from the influence of the shorter branch. As seen in the figure, the retardation behavior is misleadingly similar to closure-related effects, even though no closure is present in that case.

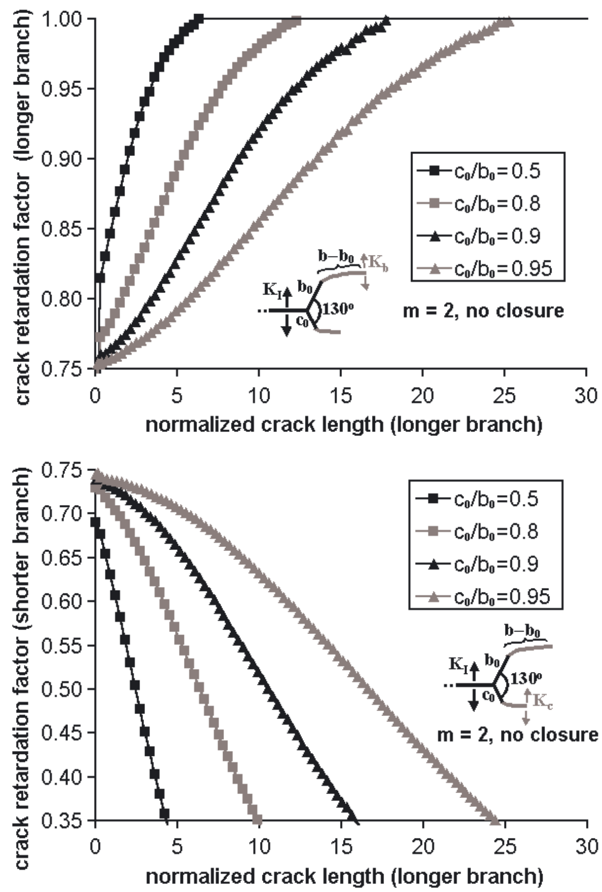

Figure 10. Normalized equivalent SIF for the longer (top) and shorter (bottom) branches of a bifurcated crack during its propagation ($2\theta = 130^o$, m = 2).

In addition, as the length difference between both branches increases, it is expected that the propagation rate of the shorter one is reduced until it arrests, after which the larger branch will dominate. Note that even small differences between the branch lengths (such as in the case $c_0/b_0 = 0.95$ shown in Figure 10) are sufficient to cause subsequent arrest of the shorter branch.

Figure 11 shows the effect of the bifurcation angle 2θ on the retardation factor K_b/K_I for $c_0/b_0 = 0.9$ and m = 3. Note that the retardation effect lasts longer for larger bifurcation angles, not only because the associated Mode I SIF is smaller, but also because the shielding effect is weaker since both branch tips are further apart, delaying the arrest of the shorter one.

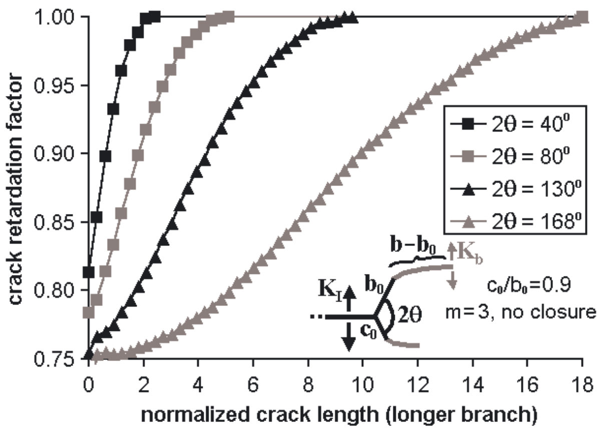

Figure 11. Normalized SIF K_b/K_I of the longer branch during its propagation as a function of the normalized length $(b–b_0)/b_0$ for $c_0/b_0 = 0.9$, m = 3.

An empirical expression is here proposed to model the SIF K_b of the longer branch during the transition between K_{b0} (immediately after the bifurcation event) and the straight-crack K_I (after the end of the retardation effect), valid for $b_0 \leq b \leq b_f$ and $0.7 < c_0/b_0 < 1$:

$$K_b = K_{b0} + (K_I - K_{b0}) \cdot \left[\operatorname{atan}\left(3 \frac{b - b_0}{b_f - b_0} \right) / 1.25 \right]^{2c_0/b_0} \quad (14)$$

Note that all proposed empirical equations are, at least in theory, applicable to any bifurcated crack in any specimen, provided that the crack branches are small if compared to the specimen geometry and that the propagation behavior of the material can be described using Equation (11). It must be pointed out, however, that the presented FE results and empirical models might have some limitations, because actual bifurcations can be of a size comparable to the scale of local plasticity (e.g. the plastic zone size) or microstructural features (e.g. grain size). Moreover, possible closure and environmental effects should be considered when comparing the bifurcation model predictions with measured crack growth rates [2].

CONCLUSIONS

In this work, a specialized FE program was used to calculate the propagation path and associated stress intensity factors (SIF) of kinked and bifurcated cracks, which can cause crack retardation or even arrest. Several crack propagation simulations were obtained to fit empirical equations to the process zone size and crack retardation factor along the curved crack path. In particular, the bifurcation simulations included several combinations of bifurcation angles $2\theta = \{40^o, 80^o, 90^o, 130^o, 168^o\}$, branch asymmetry ratios $c_0/b_0 = \{0.5, 0.7, 0.8, 0.9, 0.95, 1.0\}$, and crack growth exponents m = {2, 3, 4}

It was found that crack bifurcation can reduce the SIF to about 0.63 of its original value, however soon after the branches start propagating this value stabilizes at 0.75 as long as the branches are approximately symmetrical. It was also shown that very small differences between the lengths of the bifurcated branches are sufficient to cause the shorter one to eventually arrest as the longer branch returns to the pre-overload propagation conditions. The process zone size was found to be smaller for lower bifurcation angles and for branches with greater asymmetry, in both cases due to the increased shielding effects on the shorter branch. The retardation zone was reduced as well for materials with higher crack growth exponents, due to the increased difference between the crack growth rates of the longer and shorter branches.

The proposed equations, besides capturing all above described phenomena, can be readily used to predict the propagation behavior of branched and kinked cracks in an arbitrary structure, as long as the process zone is small compared to the other characteristic dimensions. From these results, it was shown that crack bifurcation may provide an alternate mechanistic explanation for overload-induced crack retardation, in special to explain load interaction effects under (closure-free) high R ratios.

It should be recognized however that the presented mixed-mode equations are only accurate if the kink length greatly exceeds the size scale of the microstructural inhomogeneities and the size of the near-tip plastic zone. But assuming that the entire crack-front deflects uniformly, the specimen thickness itself may provide the size scale requirements for the validity of the presented equations, as the calculated SIF may be averaged considering the (several) grains present along the thickness. Otherwise, if the crack deflections vary significantly along the thickness, then further modeling including Mode III effects should be considered.

REFERENCES

[1] Lankford, J., Davidson, D.L. “The Effect of Overloads upon Fatigue Crack Tip Opening Displacement and Crack Tip Opening/Closing Loads in Aluminum Alloys,” in Advances In Fracture Research, Pergamon Press, v.2, pp.899-906, 1981.

[2] Suresh, S. “Crack Deflection: Implications for the Growth of Long and Short Fatigue Cracks,” Metallurgical Transactions, v.14a, pp.2375-85, 1983.

[3] Kosec, B., Kovacic, G., Kosec, L. “Fatigue Cracking of an Aircraft Wheel,” Engineering Failure Analysis, v.9, pp.603-9, 2002.

[4] Suresh, S. “Micromechanisms of Fatigue Crack Growth Retardation Following Overloads,” Engin. Fracture Mechanics, v.18, n.3, pp.577-93, 1983.

[5] Suresh, S. “Fatigue of Materials,” ISBN 0-521-57847-7, Cambridge University Press, 1998, 679p.

[6] Seelig, T., Gross, D. “On the Interaction and Branching of Fast Running Cracks - A Numerical Investigation,” Journal of the Mechanics and Physics of Solids, v.47, pp.935-52, 1999.

[7] Karihaloo, B.L. “On Crack Kinking and Curving,” Mechanics of Materials, v.1, pp.189-201, 1982.

[8] Suresh, S., Shih, C.F. “Plastic Near-tip Fields for Branched Cracks”, International Journal of Fracture Vol.30, pp.237-259, 1986.

[9] Miranda, A.C.O., Meggiolaro, M.A., Castro, J.T.P., Martha, L.F., Bittencourt, T.N. “Fatigue Crack Propagation under Complex Loading in Arbitrary 2D Geometries,” in Braun AA, McKeighan PC, Lohr RD, Editors, Applications of Automation Technology in Fatigue and Fracture Testing and Analysis, ASTM STP 1411, v.4, pp.120-46, 2002.

[10] Meggiolaro, M.A., Castro, J.T.P. “ViDa - Danometro Visual para Automatizar o Projeto à Fadiga sob Carregamentos Complexos,” Journal of the Brazilian Society of Mechanical Sciences, v.20, n.4, pp.666-85, 1998 (in Portuguese).

[11] Shih, C.F., de Lorenzi, H.G., German, M.D. “Crack Extension Modeling with Singular Quadratic Isoparametric Elements,” International Journal of Fracture, v.12, pp.647-51, 1976.

[12] Raju, I.S. “Calculation of Strain-Energy Release Rates with Higher Order and Singular Finite Elements,” Engineering Fracture Mechanics, v.28, pp.251-74, 1987.

[13] Rybicki, E.F., Kanninen, M.F. “A Finite Element Calculation of Stress-Intensity Factors by a Modified Crack Closure Integral,” Engineering Fracture Mechanics, v.9, pp.931-938, 1977.

[14] Dodds, R.H. Jr., Vargas, P.M. “Numerical Evaluation of Domain and Contour Integrals for Nonlinear Fracture Mechanics,” Report, Dept. of Civil Engineering, Univ. of Illinois, Urbana-Champaign, 1988.

[15] Nikishkov, G.P., Atluri, S.N. “Calculation of Fracture Mechanics Parameters for an Arbitrary Three-Dimensional Crack by the Equivalent Domain Integral Method,” International Journal for Numerical Methods in Engineering, v.24, pp.1801-21, 1987.

[16] Bittencourt, T.N., Wawrzynek, P.A., Ingraffea, A.R., Sousa, J.L.A. “Quasi-Automatic Simulation of Crack Propagation for 2D LEFM Problems,” Engineering Fracture Mechanics, v.55, pp.321-34, 1996.

[17] McEvily, A.J. “Current Aspects of Fatigue”, Metal Science, v.11, pp.274-84, 1977.

[18] Tanaka, K., “Fatigue Propagation from a Crack Inclined to the Cyclic Tensile Axis,” Engineering Fracture Mechanics, v.6, pp.493-507, 1974.

[19] Hussain, M.A., Pu, S.U., Underwood, J. “Strain Energy Release Rate for a Crack under Combined Mode I and II,” ASTM STP 560, pp.2-28, 1974.

[20] Sih, G.C. “Strain-Energy-Density Factor Applied to Mixed Mode Crack Problems,” International Journal of Fracture Mechanics, v.10, pp.305-321, 1974.

[21] Erdogan, F., Sih, G.C. “On the Crack Extension in Plates under Plane Loading and Transverse Shear,” Journal of Basic Engineering, v.85, pp.519-27, 1963.

[22] Pippan, R., Flechsig, K., Riemelmoser, F.O. “Fatigue Crack Propagation Behavior in the Vicinity of an Interface between Materials with Different Yield Stresses,” Materials Science and Engineering, v.A283, pp.225-33, 2000.

[23] Miranda, A.C.O., Meggiolaro, M.A., Castro, J.T.P., Martha, L.F., Bittencourt, T.N. “Fatigue Life and Crack Path Prediction in Generic 2D Structural Components,” Engineering Fracture Mechanics, v.70, pp.1259-1279, 2003.

[24] Cotterell, B., Rice, J.R. “Slightly Curved or Kinked Cracks,” International Journal of Fracture, v.16, pp.155-69, 1980.

[25] Lo, K.K. “Analysis of Branched Cracks,” Journal of Applied Mechanics, v.45, pp.797-802, 1978.

[26] Shi, H.J., Niu, L.S., Mesmacque, G., Wang, Z.G. “Branched Crack Growth Behavior of Mixed-Mode Fatigue for an Austenitic 304L Steel,” International Journal of Fatigue, v.22, pp.457-65, 2000.